RSC Advances

PAPER

View Article Online
View Journal | View Issue

Solution processed sun baked electrode material for flexible supercapacitors†

Cite this: *RSC Adv.*, 2014, **4**, 20281

Narendra Kurra,‡ S. Kiruthika‡ and Giridhar U. Kulkarni*

Received 10th February 2014
Accepted 15th April 2014

DOI: 10.1039/c4ra02934h

www.rsc.org/advances

We report a new strategy for making electrode materials for supercapacitors based on a nanocrystalline Pd/carbon (nc-Pd/C) composite, obtained by thermolyzing a thin film of Pd hexadecylthiolate under sunlight. Thus obtained nc-Pd/C composite is porous (BET specific surface area, 67 $m^2\ g^{-1}$), hydrophilic (contact angle, 49°) and of good electrical conductivity (resistivity ~ 2 μΩ m), all these properties being highly suitable for supercapacitor electrodes. The autocatalytic nature of the nc-Pd/C composite was exploited for electrolessly depositing MnO_2 bearing a nanowall morphology to serve as a pseudocapacitive material. Using MnO_2/nc-Pd/C electrodes in 1 M Na_2SO_4, a specific capacitance of ~450 F g^{-1} was obtained at 10 mV s^{-1}. An asymmetric supercapacitor was fabricated by employing MnO_2/nc-Pd/C as a positive electrode and nc-Pd/C as a negative electrode, where the potential window could be enhanced to 1.8 V with an energy density of 86 W h kg^{-1}. The electrode precursor being a direct write lithography resist allowed fabrication of a planar micro-supercapacitor with an ionic liquid as electrolyte, exhibiting a cell capacitance of 8 mF cm^{-2}. As our recipe does not make use of an additional charge collecting layer and binder, nor does it use any external energy during fabrication, the only cost consideration is related to Pd; however, given the extremely small amount of Pd consumed per device (~0.18 mg), it is highly cost effective.

Introduction

There is a great deal of interest worldwide in developing electrochemical energy storage devices with the aim of achieving high energy and power densities.[1–3] Conventionally, batteries and fuel cells work based on Faradaic processes[4] with high energy density (~10 to 200 W h kg^{-1}), but suffer from low power densities, low cyclability and discharge rates.[3–6] To circumvent these problems, alternative energy storage devices with higher power densities are being developed in the form of electrochemical capacitors or supercapacitors.[6–9] Besides power density, long cycle life and fast discharge rates have made supercapacitors quite attractive in recent times.[1,7–9] Basic designs of supercapacitors typically employ electrodes made of highly porous carbon based materials sometimes with pseudocapacitive coatings, with aqueous, organic or ionic liquids as electrolytes in a two or a three electrode configuration.

The capacitance of a supercapacitor is superior to that of conventional capacitor due to the formation of electrical double layer (EDL) where the ions from the electrolyte get accumulated at the electrode–electrolyte interface on applying potential.[3,10,11] The electrode material used in a supercapacitor should therefore be electrically well conducting and possess high specific surface area. These properties make an electrode accumulate large amount of charge in the EDL which can be harnessed in an external circuit.[1,3,10,11] In this context, carbon based materials have been explored extensively due to their tunable surface area, high electrical conductivity and excellent electrochemical stability, essential for a supercapacitor electrode.[12–15] Carbon materials can be activated through chemical, thermal and plasma methods[16–19] to enhance porosity and tune the morphology. Thus, activated carbon in the form of nano onions,[20] nanoparticles,[21] fibres[22] and nanotubes[23] have been employed as electrode materials for building supercapacitors. Similarly, graphene and its derivatives like curved,[24] activated,[25] solvated,[26] doped graphene[27] as well as three dimensional graphene networks,[28] have been utilized as electrode material in supercapacitors. It was found that the graphene layers tend to restack themselves with increasing number of cycles and this issue has been addressed by mixing spacers such as carbon nanotubes (CNTs) and Au nanoparticles.[29,30] Here we introduce a supercapacitor electrode material consisting of nanocrystalline Pd in

Chemistry & Physics of Materials Unit and Thematic Unit of Excellence on Nanochemistry, Jawaharlal Nehru Centre for Advanced Scientific Research, Jakkur P.O., Bangalore 560 064, India. E-mail: kulkarni@jncasr.ac.in; Fax: +91 (80) 22082766; Tel: +91 (80) 22082814

† Electronic supplementary information (ESI) available: Schematic of hot plate thermolysis (Fig. S1), particle size analysis from XRD peak fitting (Fig. S2), optical profiler image of nc-Pd/C film (Fig. S3), CV in two & three electrode configuration (Fig. S4), XPS, SEM, coverage analysis and CV of MnO_2 coated electrodes (Fig. S5–S8), IR drop calculation (Fig. S9), CV of asymmetric electrodes (Fig. S10), impedance measurements (Fig. S11), Optical microscopy image of micro-supercapacitor (Fig. S12), calculations of energy & power density, Table S1 and Note S1. Solar baking of precursor is shown in Movie 1. See DOI: 10.1039/c4ra02934h

‡ These authors have contributed equally.

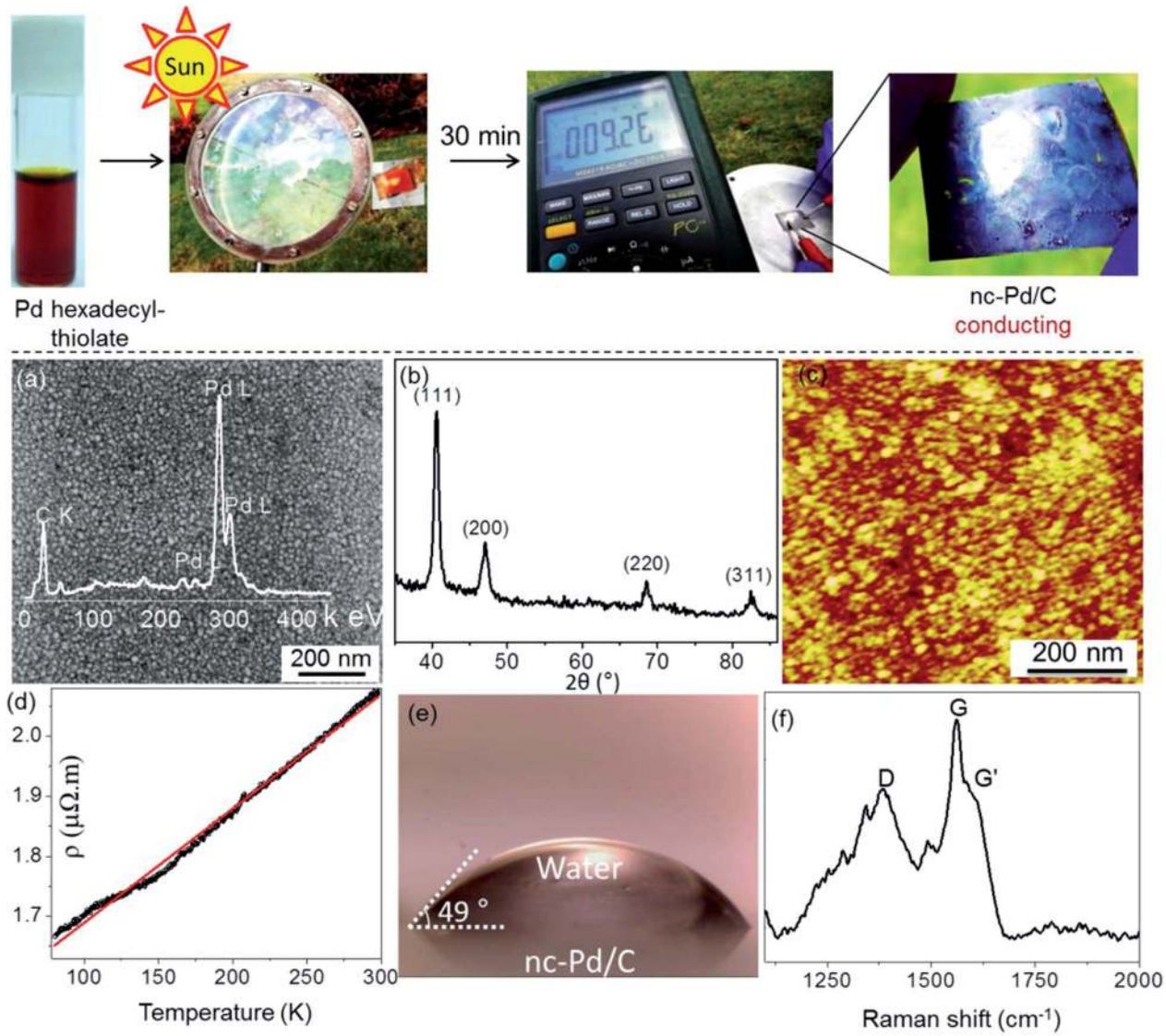

Fig. 1 Photograph showing solution processable metal–organic precursor, Pd hexadecylthiolate. Thermolysis of Pd hexadecylthiolate (orange color) into nc-Pd/C (black color) after annealing under sunlight. Focussed spot of sunlight on the sample surface along with the lens is shown. Multimeter displaying the resistance value of the nc-Pd/C composite film which is conducting following thermolysis. (a) FESEM image showing the densely packed Pd nanoparticles, inset is the energy dispersive spectrum (EDS) showing Pd L and C K signals. (b) XRD of nc-Pd/C composite film. The indexed peaks are matching well with metallic Pd. (c) AFM topography of the nc-Pd/C film. (d) Temperature dependent resistivity of the film showing near metallic behavior. (e) Water contact angle of the nc-Pd/C film, indicating hydrophilic nature of the surface. (f) Raman spectrum of the nc-Pd/C film showing the presence of functionalized amorphous carbon.

carbon matrix (nc-Pd/C) derived from controlled decomposition of a molecular precursor under sunlight.

The major challenge is to improve the energy density of a supercapacitor without sacrificing its power density. This has intensified the search for novel electrode materials with tailored material composition, size and morphology, to go with a range of electrolytes.[3,31] As the energy density (E) is proportional to the specific capacitance (C_i) and square of the operating potential window (V), given by the following eqn (1).

$$E = 1/2C_iV^2 \quad (1)$$

E can be enhanced by increasing C_i and V. The specific capacitance of supercapacitors has been improved by employing pseudocapacitive coatings such as transition metal oxides[32–35] and conducting polymers[36,37] which is due to fast and reversible redox reactions near the surface of active materials. However, the maximum stable potential window of aqueous electrolytes is only 1.23 V, the potential window can be increased by employing organic electrolytes but they suffer from high cost, toxicity and poor conductivity.[10] Hence, the potential window of green electrolytes (aqueous based) can be increased through designing asymmetric supercapacitors (ASCs) which employ a combination of battery-like Faradic electrode (as energy source) and a capacitive electrode (as power source) to achieve high energy density.[38,39] Due to its low cost and non-toxicity, MnO_2 (theoretical specific capacitance ~1370 F g^{-1})

has been widely employed as a pseudocapacitive material in combination with high surface area electrodes.[40–43]

Supercapacitors based on carbon materials and pseudocapacitive coatings involve high temperature treatments, activation by chemicals, multi-step complex solution processing and chemical vapor deposition techniques.[16–39] Implementation with additives such as polymer binders and conductive adhesives may increase the mechanical stability of the electrode materials but often cause degradation of the electrochemical performance.[30–35] Addressing these issues, recently, Wei *et al.*, have fabricated thin activated carbon film electrode based supercapacitor obtained through carbonization and activation using temperatures above 700 °C.[44] Processing of highly conducting carbon based thin films at lower temperatures could offer new capabilities in making on-chip energy storage devices. Thus, the quest is to arrive at an optimized electrode material involving simple and solution processable chemical recipes in a binder-free manner. Here, we use a novel metal–organic precursor for obtaining Pd nanoparticles embedded in conducting carbon films through a solution processable route combined with thermolysis at just about 220 °C, using sunlight. The autocatalytic nature of this composite was realised through the spontaneous reduction of permanganate ions into insoluble MnO_2 with nanowall morphology, confirmed through Raman and SEM analysis. Using nc-Pd/C and MnO_2 deposited electrodes (MnO_2/nc-Pd/C), we have been able to fabricate symmetric and asymmetric supercapacitors which exhibited electrochemical performance, comparable or sometimes superior to many carbon based supercapacitors. Using direct write e-beam lithography, the fabrication was extended to realise planar micro-supercapacitors.

Results and discussion

Pd hexadecylthiolate is a novel precursor which upon mild thermolysis, produces nanocrystalline Pd in carbon matrix (nc-Pd/C) with tunable conducting property.[45] The precursor is amenable for patterning by various lithography techniques to achieve fine features of the nc-Pd/C.[46–49] This composite was previously employed in our laboratory as an active material in fabricating hydrogen[47] and strain sensors.[45] In this study, we have fabricated supercapacitors by employing nc-Pd/C composite as conducting electrode, importantly, by carrying out the thermolysis of the precursor under sunlight. Pd hexadecylthiolate precursor was drop coated on a glass or quartz substrate and allowed to dry in air to give rise to an orange colored film which was poorly conducting. The dried film was brought under a lens focusing the sunlight such that the local temperature reached ~220 °C when the film began to release volatile carbonaceous species and turned into a dark colored film (see ESI, Movie 1†). It became highly conducting as shown on the right side of the schematic in Fig. 1. The film has been characterized in detail (Fig. 1a–e). It is essentially a nanocrystalline film with particle size of 15–20 nm as seen from the FESEM image in Fig. 1a. The EDS spectrum showed the presence of Pd and C in the ratio ~40 : 60 at%. It is evident that the Pd hexadecylthiolate underwent decomposition leading to the formation of the Pd nanoparticles along with the carbonaceous species. The XRD pattern of the film showed peaks corresponding to metallic Pd with the estimated particle size of ~16 nm (Fig. 1b and ESI, Fig. S2†). The measured roughness from AFM image in Fig. 1c was 1.13 nm, which is in the acceptable range for a planar electrode. The thickness of the film was measured to be ~300 nm (ESI, Fig. S3†). The room temperature resistivity of the film was found to be ~2 μΩ m, which decreased nearly linearly with temperature exhibiting metallic type behavior (Fig. 1d). Thus, the sun baked nc-Pd/C composite film exhibited essential requisites of an electrode. Further, the water contact angle was only 49° (Fig. 1e), an important property for use with aqueous electrolyte. The Raman spectrum showed the presence of a broad D (position, 1377 cm^{-1}, width, 185 cm^{-1}) and G bands (1564 cm^{-1}, 38 cm^{-1}) with a shoulder at 1620 cm^{-1} corresponding to the G′ band (width ~55 cm^{-1}), implying the presence of functionalized amorphous carbon (see Fig. 1f).[45] The latter may be expected to enhance water wettability. Using nc-Pd/C composite, several supercapacitor devices of varied designs were made (see Table 1).

Table 1 A list of supercapacitor devices fabricated in this study

No.	Supercapacitor	Configuration	MnO_2 deposition (min)	Electrolyte	C_i (F g^{-1}) at 10 mV s^{-1}	More details in Figure	Other details
1	nc-Pd/C	Symmetric	—	1 M Na_2SO_4	142	2 & 6	S2–S4 & S11†
2	MnO_2/nc-Pd/C	Symmetric	0.5	1 M Na_2SO_4	157	3 & S8a†	S6a†
3	MnO_2/nc-Pd/C	Symmetric	1	1 M Na_2SO_4	190	3 & S8b†	S6b†
4	MnO_2/nc-Pd/C	Symmetric	2	1 M Na_2SO_4	452	3 & 6	S5, S6c, S6f, S7, S9 & S11†
5	MnO_2/nc-Pd/C	Symmetric	5	1 M Na_2SO_4	342	3 & S8c†	S6d†
6	MnO_2/nc-Pd/C	Symmetric	10	1 M Na_2SO_4	272	3 & S8d†	S6e†
7	MnO_2/nc-Pd/C// nc-Pd/C	Asymmetric	2	1 M Na_2SO_4	192	5, 6 & S6†	S10 and S11†
8	MnO_2/nc-Pd/C (flexible)	Symmetric	2	PVA/H_2SO_4	220	4	Kapton substrate
9	nc-Pd/C (micro-supercapacitor)	Symmetric	—	Ionic liquid	8 mF cm^{-2}	7	Si/SiO_2 (300 nm) substrate

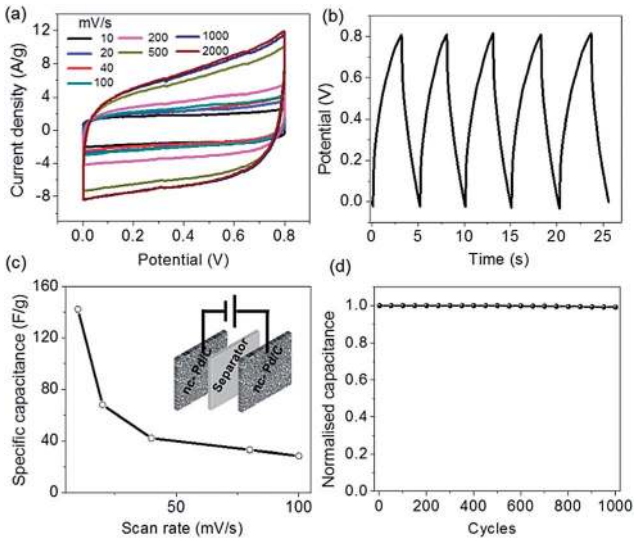

Fig. 2 The performance of the symmetric nc-Pd/C electrochemical capacitor in aqueous 1 M Na_2SO_4 solution. (a) Cyclic voltammograms (CV) at different scan rates, from 10 to 2000 mV s^{-1}. (b) Galvanostatic charge–discharge (CD) curves at a current density of 5 A g^{-1}. (c) Specific capacitance as a function of scan rate, inset shows the two-electrode configuration of the symmetric nc-Pd/C electrodes along with the separator. (d) Normalized capacitance *vs.* number of cycles showing the electrochemical stability of nc-Pd/C electrodes over 1000 cycles (data points corresponding to every 50th cycle, are shown).

Firstly, a symmetric supercapacitor was assembled using two nc-Pd/C electrodes separated by a filter paper and in 1 M Na_2SO_4 as aqueous electrolyte (5 mL). The electrochemical performance of the device was examined by cyclic voltammetry (CV) and galvanostatic charge–discharge (CD) measurements (Fig. 2). The CV curves are nearly rectangular in shape over scan rates of 10–2000 mV s^{-1} in the potential window of 0–0.8 V, indicating clearly the formation of EDL (Fig. 2a). When the CV measurement was carried out in 3-electrode configuration (ESI, Fig. S4†), the current density was somewhat higher as one would expect.[10] The CD curves measured in the potential window of 0–0.8 V at a current density of 5 A g^{-1} (Fig. 2b), showed nearly triangular shape reflecting efficient EDL at the electrode–electrolyte interface.

The specific capacitance of ~140 F g^{-1} (areal capacitance of 56 mF cm^{-2}) was estimated at a low scan rate of 10 mV s^{-1} which was found to decrease with increasing scan rate (Fig. 2c). The drop of specific capacitance at higher scan rates is due to mesoporous nature of the sample with limited diffusion rate of ions. Using typical value for EDL capacitance as ~0.3 F m^{-2},[10] the electrochemical active specific surface area was estimated to be 466 m^2 g^{-1}. Compared to BET value, the latter may be more appropriate particularly for thin film supercapacitors.[50] The capacitance retention test conducted over 1000 cycles demonstrated excellent electrochemical stability of the device and hence the nc-Pd/C electrodes (Fig. 2d).

The autocatalytic nature of the nc-Pd/C composite was exploited for spontaneous deposition of MnO_2 by dipping in neutral permanganate solution. MnO_4^- ions could be reduced to MnO_2 on functionalized nc-Pd/C surfaces based on reaction (2).[51,52]

$$4MnO_4^- + 3C + H_2O \rightarrow 4MnO_2 + CO_3^{2-} + 2HCO_3^- \quad (2)$$

$$MnO_4^- + 4H^+ + 3e^- \rightarrow MnO_2 + 2H_2O \quad (3)$$

Reduction of permanganate ion (MnO_4^-) to MnO_2 on carbon surfaces is pH dependent. Typically, protons and electrons are required for the reduction of permanganate into MnO_2 according to the eqn (3). In the case of graphitic materials such as carbon nanotubes and graphene, the surfaces have to be treated with acid solutions in order to functionalize for reduction of permanganate into MnO_2. As nc-Pd/C composite is conducting and contains functionalized carbon, the surface offers plenty of reduction sites for the permanganate ions to get reduced to MnO_2. Earlier, it has been shown that the nc-Pd/C surface exhibits autocatalytic property which could assist the spontaneous growth of Cu, ZnO and polyaniline.[53,54] X-ray photoelectron spectroscopy (XPS) analysis has shown facile deposition of MnO_2 on nc-Pd/C film (ESI, Fig. S5†). Thus grown MnO_2 exhibits nanowall-like morphology suitable for EDLs and pseudocapacitive behavior (ESI, Fig. S6†). The typical width of the nanowalls was found to be 20–30 nm and height, 30–50 nm for a surface coverage of 36% (ESI, Fig. S7†). The electrolyte ions can thus access the entire surface of the vertical MnO_2 walls which should lead to enhanced capacitance. The amount of MnO_2 deposited on the nc-Pd/C surface was controlled by the dipping time (30 second to 10 minutes) in permanganate solution. Fig. 3a shows the scan rate dependent CVs for a symmetric supercapacitor with 2 minutes deposited MnO_2 (scan rates of 10–200 mV s^{-1} and potential window, 0–0.8 V). The electrochemical performance of the MnO_2/nc-Pd/C electrodes with different loadings of MnO_2 (dipping times of 0.5, 1, 5 and 10 minutes) was investigated using cyclic voltammetry (ESI, Fig. S8†). We have found that the mass loading of MnO_2 obtained with 2 minutes deposition produced high current density and hence high specific capacitance compared to other loadings. The galvanostatic charge–discharge curves at different current densities (2 to 10.2 A g^{-1}) are shown in Fig. 3b. The triangular nature of the charge and discharge curves reveal the capacitive characteristics of the MnO_2/nc-Pd/C electrodes. The specific capacitance of the different loadings of MnO_2 on nc-Pd/C was plotted against the scan rate (Fig. 3c). It was found that the 2 minutes deposition showed a maximum specific capacitance of 450 F g^{-1} at a scan rate of 10 mV s^{-1}. The specific capacitance was found to increase from 140 F g^{-1} for the pristine nc-Pd/C to 450 F g^{-1} after MnO_2 deposition (2 minutes). The electrochemical active surface area for the MnO_2/nc-Pd/C architecture is found to be 1500 m^2 g^{-1} which is 3 times higher compared to planar nc-Pd/C composite film. For higher loading of MnO_2, however, the specific capacitance decreased (Fig. 3d). As MnO_2 is an insulating material, thicker deposits increase the resistivity in the film, leading to the decreased specific capacitance. An optimal coverage of MnO_2 over the nc-Pd/C is required for obtaining better performance which under the conditions employed was found to be ~2 minutes. The equivalent series

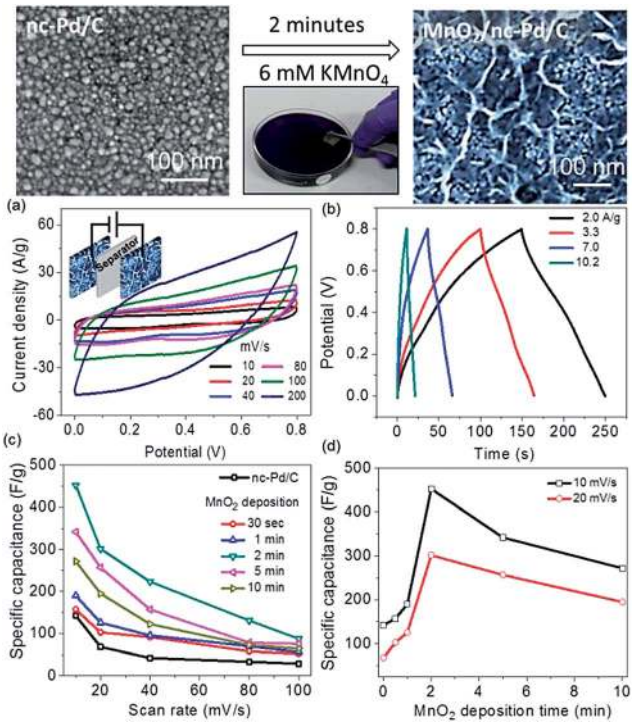

Fig. 3 The process of depositing MnO_2 on the nc-Pd/C electrode is shown in top schematic. (a) Cyclic voltammetry curves for (2 minutes) MnO_2/nc-Pd/C symmetric supercapacitor at different scan rates ranging from 10 to 200 mV s^{-1} (electrolyte used, 1 M Na_2SO_4). Inset shows the schematic of the supercapacitor cell. (b) Galvanostatic charging–discharging curves at different current densities. (c) Specific capacitance *versus* scan rates for varied mass loadings of MnO_2 in comparison to nc-Pd/C. (d) Plot of specific capacitance with respect to MnO_2 deposition times at scan rates of 10 and 20 mV s^{-1}.

resistance (ESR) calculated from the IR drop in the discharge curve was found to be 16 Ω (ESI, Fig. S9†).

Flexible solid state symmetric supercapacitors were also made using MnO_2/nc-Pd/C electrodes, by forming the MnO_2/nc-Pd/C composite film on Kapton sheets instead of glass. We have not employed metallic films or foams as current collectors which are typically rigid and inflexible. The nc-Pd/C film, besides being flexible, is itself a good current collector. The flexibility of nc-Pd/C composite film was tested for 1000 bending cycles (bending radius = 3 mm), which showed resistance variation of 5%, thus qualifying it as a flexible composite film (Fig. 4a). As made supercapacitor device was flexible, bendable and also foldable. The CV curves remain same as that of planar device even after bending for several times (Fig. 4b).

Following eqn (1), the energy density can be enhanced by increasing the potential window. This was achieved by making an asymmetric configuration of the electrodes. In the asymmetric configuration (ASC), the MnO_2/nc-Pd/C//nc-Pd/C electrodes were connected to the positive and negative terminals respectively in 1 M Na_2SO_4 solution. The CV curves obtained at different scan rates for MnO_2/nc-Pd/C//nc-Pd/C device (potential window, 0–0.8 V) showed rectangular curves, indicative of the capacitive behavior of the ASC cell (Fig. 5a). Further, the CV curves could also be recorded with extended potential range upto 1.8 V, indicating the stable nature of the ASC (Fig. 5b, ESI, Fig. S10†). The specific capacitance increased significantly, from 112 to 194 F g^{-1} as the potential increased from 0.8 to 1.8 V (Fig. 5c). An ASC thus minimises the number of serially connecting devices to derive the desired output voltage. The electrochemical stability of the ASC was tested by doing charge–discharge cycles over 1000 times at a current density of 7 A g^{-1} (Fig. 5d). The impedance data of symmetric nc-Pd/C, MnO_2/nc-Pd/C and asymmetric supercapacitors (MnO_2/nc-Pd/C//nc-Pd/C) have been compared and were found to be similar indicating that even after deposition of insulating MnO_2 nanowalls, the electron transfer kinetics remained unaltered thanks to

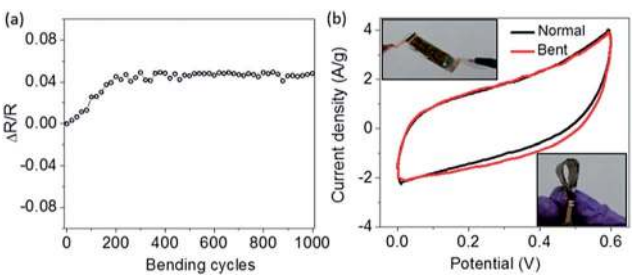

Fig. 4 (a) Flexibility of the nc-Pd/C composite film over 1000 cycles. Normalized change resistance with respect to bending cycles, only 5% variation in the resistance is observed during the bending experiments. (b) CV curves for the flat and bent configurations of the device at a scan rate of 20 mV s^{-1} (electrolyte used, PVA/H_2SO_4 gel). Inset shows the photograph of a flexible MnO_2/nc-Pd/C solid state symmetric supercapacitor, both in planar and bent geometries.

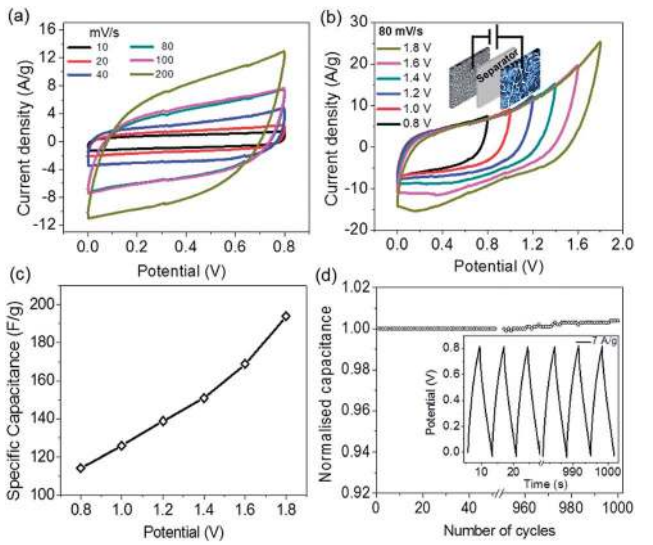

Fig. 5 (a) CV curves of (2 minutes) MnO_2/nc-Pd/C//nc-Pd/C asymmetric supercapacitor (ASC) measured at different scan rates between 0 and 0.8 V. (b) CV curves of the ASC measured at different potential windows at a scan rate of 80 mV s^{-1}. (c) Specific capacitances of the ASC obtained for increasing potential window at a scan rate of 80 mV s^{-1}. (d) Cycling stability of the ASC over 1000 cycles of charge–discharge cycles at a current density of 7 A g^{-1}. Inset shows the charge–discharge curves of the device.

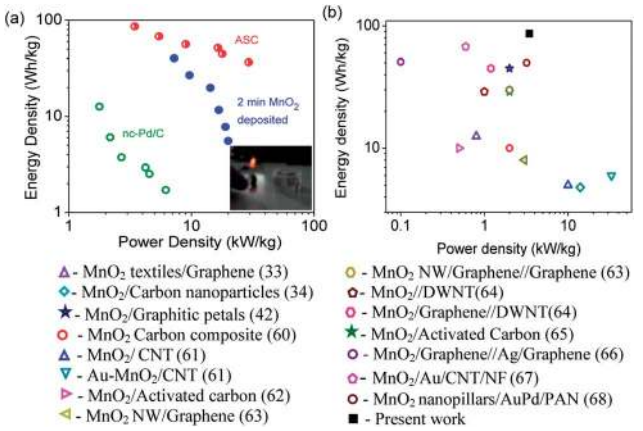

Fig. 6 Ragone plots for the nc-Pd/C, MnO_2/nc-Pd/C and MnO_2/nc-Pd/C//nc-Pd/C ASC in 1 M Na_2SO_4. Inset shows the glowing red LED after connecting to the three cells in series. (b) Ragone plot comparing a ASC from this study with various MnO_2 coated carbon based supercapacitors from the literature (reference number is mentioned in brackets).

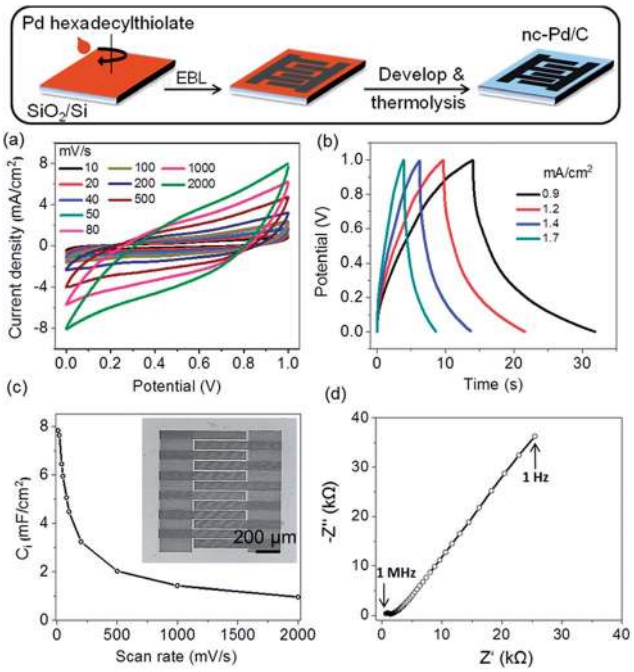

Fig. 7 Micro-supercapacitors based on nc-Pd/C composite. Schematic shows the fabrication of micro electrodes of nc-Pd/C through electron beam lithography of Pd hexadecylthiolate. (a) CV curves of the nc-Pd/C micro-supercapacitor at different scan rates. (b) Charge–discharge cycles at different current densities. (c) Specific capacitance *vs.* scan rate of the micro-supercapacitor. Inset shows the optical micrograph of interdigitated nc-Pd/C electrodes. (d) Nyquist plot for the micro-supercapacitor recorded from 1 Hz to 1 MHz.

favorable interfacial contact resistance between MnO_2 and nc-Pd/C (ESI, Fig. S11†).

The electrochemical performances of the different supercapacitors are depicted in the form of Ragone plot in Fig. 6 (for details of the calculations, see ESI, Table S1†). The energy density is seen to decrease for increasing power density for all the devices. The MnO_2 based supercapacitors perform better than those which simply use nc-Pd/C electrodes. Among all, the MnO_2/nc-Pd/C//nc-Pd/C ASCs exhibit the highest energy densities in the given range of power density much higher than the commercially available supercapacitor devices (energy density, $\sim$10 W h kg^{-1} and power density, $\sim$10 kW kg^{-1}), which are mostly based on porous carbon.[21] The performance obtained in this study may also be compared with MnO_2 coated carbon based supercapacitors reported in the literature as shown in Fig. 6b. The inset of Fig. 6a is a demonstration of the glowing of a 1.5 V LED by the ASC. Serially connected 3 ASCs (each 1 $\times$ 2.5 cm^2) charged at 1.5 V for 30 seconds were used for glowing the LED for $\sim$2 minutes.

Micro-supercapacitors is an emerging area of research with potential applications as micropower devices in many fields such as RFID tags, ac-line filtering and as often such devices are realized in planar geometry.[55–58] As Pd hexadecylthiolate is amenable for patterning,[45–48] we have employed electron beam lithography to fabricate interdigitated nc-Pd/C electrodes on a SiO_2/Si substrate. Patterning of interdigitated planar electrodes could be useful for improved kinetic performance due to a shortened diffusion length.[17,20] Interdigitated electrodes (width, 65 μm; length $\sim$350 μm with a spacing of $\sim$10 μm) were fabricated by exposing a thin film of Pd hexadecylthiolate ($\sim$500 nm) at an e-dosage of 50 μC cm^{-2} followed by developing in toluene for 10 seconds. Thus obtained patterns were thermolysed at 220 °C for 3 h which resulted in the formation of conducting nc-Pd/C electrodes in a planar geometry (schematic Fig. 7). An ionic liquid (1-butyl-3-methylimidazolium methylsulfate) was employed as an electrolyte due to its low vapor pressure. The CV curves were nearly rectangular even at high scan rate of 2000 mV s^{-1} (see Fig. 7a). The charge–discharge cycles were recorded at different current densities (0.9–1.7 mA cm^{-2}) which were triangular in shape due to efficient EDLs that were formed in the micro nc-Pd/C electrodes (Fig. 7b). The cell capacitance, calculated based on the total area of the electrode pads, found to be 8 mF cm^{-2} at a scan rate of 10 mV s^{-1} (Fig. 7c). Micro-supercapacitors based on carbon materials have shown typical values of 0.4–2 mF cm^{-2}.[20] The inset in Fig. 7c shows SEM image of the fabricated interdigitated electrode, while optical microscopy image of the device with the contacts is given in ESI, Fig. S12.† The ESR value for the fabricated micro-supercapacitor was found to be $\sim$600 Ω. The Nyquist plot showed a small semicircle in the high frequency region which is due to charge transfer resistance[10] and linear behavior in the low frequency range, indicative of capacitive behavior of the micro-supercapacitor (Fig. 7d).

It may be worthwhile to mention few merits of the nc-Pd/C composites as electrodes for designing the sandwich and planar supercapacitors. This method offers a way to fabricate the metal nanoparticle–carbon composites *via* solution processable route in which the decomposition of the metal–organic precursors leads to the nucleation of Pd nanoparticles along with functionalized carbon. Thus formed composite is highly conducting while being porous, enabling facile formation of EDLs. The

functionalized nature of the carbon matrix enhances electrolyte wetting, a factor crucial for efficient transfer of charges across the electrode–electrolyte interface. Further, the autocatalytic nature of the nc-Pd/C surface facilitates spontaneous growth of MnO_2; other pseudocapacitive materials such as ZnO and polyaniline can also be deposited. Additional advantage is that the precursor employed requires moderate thermolysis temperature (<250 °C) which is easily achievable; using sunlight for this purpose is shown to be an attractive option. The performance of the electrode material can be improved *via* patterning of the metal organic precursor (which is amenable for patterning by various methods). It should also possible to fabricate planar micro-supercapacitors with pseudocapacitive materials (ZnO, PANI, *etc.*) coated on interdigitated nc-Pd/C electrodes. It may also be noted that the device performances obtained in this study are commendable albeit using two electrode configuration; performance measured employing three electrode configuration usually projects relatively higher values of capacitance.[59] Another noteworthy point is that the amount of Pd used per device is extremely small (see ESI, Note S1†). There are many advantages which are in favour of the recipe such as no additional charge collecting layer or binder is required and the electrode material preparation uses only sunlight and no other heat source.

Conclusions

In conclusion, a new strategy for making electrode material in the form of conducting nc-Pd/C composite has been developed by thermolyzing Pd hexadecylthiolate film under sunlight. The autocatalytic nature of nc-Pd/C enabled electroless deposition of pseudocapacitive MnO_2 layer within minutes. Maximum specific capacitance of 450 F g^{-1} was achieved with an optimal thickness of MnO_2. Asymmetric supercapacitors with the layer architecture, MnO_2/nc-Pd/C//nc-Pd/C, showed maximum energy density of 86 W h kg^{-1} compared to symmetric MnO_2 supercapacitor which showed ~40 W h kg^{-1}. Power densities of 20 and 30 kW kg^{-1} have been achieved for the symmetric and asymmetric supercapacitors respectively. The performance of the ASC based on MnO_2/nc-Pd/C//nc-Pd/C is found to be much higher than the commercially available activated carbon based supercapacitors. As Pd is present only in tiny amount (~0.18 mg) and as the fabrication involves no significant energy or material input, these are essentially low cost devices. By patterning the Pd precursor, planar micro-supercapacitors were also realised exhibiting cell capacitance of 8 mF cm^{-2}.

Experimental

Synthesis of nc-Pd/C composite

The synthesis procedure for the precursor, Pd hexadecylthiolate, $Pd(SC_{16}H_{33})_2$, has been reported elsewhere.[45–48] Briefly, 100 mM of 1-hexadecanethiol (Sigma Aldrich) was added to 100 mM of $Pd(OAc)_2$ (Sigma Aldrich) in toluene solution under stirring. The solution became viscous and color changed from orange to reddish orange. The glass substrates used for film formation were cleaned with deionized water and acetone followed by drying under N_2 flow. A 100 μL of 100 mM Pd hexadecylthiolate precursor solution was drop casted on a cleaned glass substrate (1 × 2.5 cm^2) resulting in an orange colored film. A convex lens with diameter of 20 cm and a focal length of 50 cm was used for concentrating the sunlight to a spot diameter of 1 cm to reach a temperature of ~220 °C on the film, measured using a thermometer. During the heat treatment, the precursor decomposes leading to the formation of conducting nc-Pd/C composite within 30 minutes. Alternatively, nc-Pd/C was also obtained through heating on a hot plate (temperature ~ 220 °C) for 3 h.

MnO_2 deposition

Neutral aqueous solution (pH = 7) of $KMnO_4$ (6 mM) was employed as a precursor solution for depositing MnO_2 nanoscale petals in an electroless manner on the autocatalytic nc-Pd/C surfaces for dipping times of 30 seconds, 1, 2, 5 and 10 minutes. The samples were thoroughly washed with distilled water in order to remove the unreacted permanganate solution followed by drying using N_2. The mass of the coated MnO_2 was calculated from the weight difference before and after the coating process. The loading amount of MnO_2 in this study is approximately 20 to 140 μg depending on the plating time, which was measured using a microbalance.

Characterization techniques

X-ray diffraction (XRD) measurements were performed using a Siemens Seifert 3000TT diffractometer (Cu Kα 1.5406 Å). Scanning electron microscopy (SEM) measurements of the nc-Pd/C films were done using a Nova NanoSEM 600 instrument (FEI Co., The Netherlands). Energy-dispersive spectroscopy (EDS) analysis was performed with an EDAX Genesis instrument (Mahwah, NJ) attached to the SEM column. AFM imaging was done on a diInnova SPM (Veeco, USA) using Si probes (model, RTESPA, spring constant 40 N m^{-1}) in tapping mode. Raman spectra were recorded on various nc-Pd/C samples in the backscattering geometry using a 532 nm excitation from a diode pumped frequency doubled Nd:YAG solid state laser (model GDLM-5015L, Photop Swutech, China) and a custom-built Raman spectrometer equipped with a SPEX TRIAX 550 monochromator and a liquid nitrogen cooled CCD detector (Spectrum One with CCD3000 controller, ISA Jobin Yvon). Temperature-dependent resistivity measurements were done using a cooling/heating stage (Linkam THMS 600) equipped with a temperature controller (Linkam TMS 94) interfaced with Keithley 236 source and measure unit. The thickness of the film was examined using a Wyko NT1100 optical profiler (Veeco, USA). X-ray photoelectron spectroscopy (XPS) measurements have been carried out using Omicron SPHERA spectrometer with nonmonochromatic AlKαX-rays (E = 1486.6 eV). ImageJ software was used to perform analysis of coverage of MnO_2 over nc-Pd/C.

Electrochemical measurements

The electrochemical properties of the nc-Pd/C films were investigated in two electrode configuration using 1 M Na_2SO_4

aqueous solution. The PVA/H_2SO_4 gel electrolyte was prepared as follows: 1 g of H_2SO_4 was added into 10 mL of deionized water, followed by 1 g of PVA powder. The whole mixture was heated to 85 °C while stirring until the solution became clear. Whatmann filter paper (pore size of 220 nm, NKK TF40, 40 μm) was used as a separator, sandwiched between two nc-Pd/C electrodes. Ionic liquid such as 1-butyl-3-methylimidazolium methylsulfate was employed as an electrolyte in the micro-supercapacitors. Cyclic voltammetry and galvanostatic charge–discharge experiments were performed on the potentiostat equipment from Technoscience Instruments (Model PG 16250) and CH Instruments 650 Electrochemical Station (Austin, TX, USA). The impedance spectra were recorded in the frequency range 0.1 Hz to 100 kHz using CH Instruments. The specific capacitance was calculated from the equation $C_s = (2/m_t)(I/s)$ where m_t is the total mass of the electrodes (0.4–0.45 mg), I is the current in mA and s is the sweep rate in mV s^{-1} ($s = dV/dt$).

Fabrication of micro-supercapacitors

50 μL of Pd hexadecylthiolate (500 mM, filtered through 200 nm millipore filter) was spin coated on SiO_2/Si substrates followed by drying of toluene solvent in air. Electron beam lithography was performed using a field-emission SEM (Nova NanoSEM 600 instrument, FEI Co., The Netherlands) at a chamber pressure of 1×10^{-6} Torr, at a working distance of 5 mm. Selected regions on the substrate were exposed to e beam dosages of 50 μC cm^{-2} at 10 kV (beam current ~ 0.64 nA) in the patterning mode. After patterning, the substrate was developed in toluene for 10 seconds followed by thermolysis at 220 °C for 3 h which results in the formation of interdigitated nc-Pd/C electrodes.

Acknowledgements

The authors thank Professor C. N. R. Rao for his encouragement. Support from the Department of Science and Technology, Government of India is gratefully acknowledged. NK and SK acknowledge CSIR and DST-INSPIRE for fellowships, respectively. GUK acknowledges the Sheikh Saqr Senior Fellowship. The authors thank Mr Kiran and Mr M. Tangi for assistance.

References

1 M. F. El-Kady, V. Strong, S. Dubin and R. B. Kaner, *Science*, 2012, **335**, 1326–1330.
2 C. Largeot, C. Portet, J. Chmiola, P.-L. Taberna, Y. Gogotsi and P. Simon, *J. Am. Chem. Soc.*, 2008, **130**, 2730–2731.
3 P. Simon and Y. Gogotsi, *Nat. Mater.*, 2008, **7**, 845–854.
4 M. Winter and R. J. Brodd, *Chem. Rev.*, 2004, **104**, 4245–4270.
5 Y. Zhu, S. Murali, M. D. Stoller, K. J. Ganesh, W. Cai, P. J. Ferreira, A. Pirkle, R. M. Wallace, K. A. Cychosz, M. Thommes, D. Su, E. A. Stach and R. S. Ruoff, *Science*, 2011, **332**, 1537–1541.
6 Y. Zhai, Y. Dou, D. Zhao, P. F. Fulvio, R. T. Mayes and S. Dai, *Adv. Mater.*, 2011, **23**, 4828–4850.
7 C. Meng, C. Liu, L. Chen, C. Hu and S. Fan, *Nano Lett.*, 2010, **10**, 4025–4031.
8 B. G. Choi, J. Hong, W. H. Hong, P. T. Hammond and H. Park, *ACS Nano*, 2011, **5**, 7205–7213.
9 J. J. Yoo, K. Balakrishnan, J. Huang, V. Meunier, B. G. Sumpter, A. Srivastava, M. Conway, A. L. Mohana Reddy, J. Yu, R. Vajtai and P. M. Ajayan, *Nano Lett.*, 2011, **11**, 1423–1427.
10 B. E. Conway, *Electrochemical Supercapacitors, Scientific, Fundamentals and Technological Applications*, Plenum, New York, 1999.
11 J. R. Miller and P. Simon, *Science*, 2008, **321**, 651–652.
12 Y. Huang, J. Liang and Y. Chen, *Small*, 2012, **8**, 1805–1834.
13 H. Nishihara and T. Kyotani, *Adv. Mater.*, 2012, **24**, 4473–4498.
14 S. L. Candelaria, Y. Shao, W. Zhou, X. Li, J. Xiao, J. G. Zhang, Y. Wang, J. Liu, J. Li and G. Cao, *Nano Energy*, 2012, **1**, 195–220.
15 G. Wang, L. Zhang and J. Zhang, *Chem. Soc. Rev.*, 2012, **41**, 797–828.
16 L. L. Zhang, X. Zhao, M. D. Stoller, Y. Zhu, H. Ji, S. Murali, Y. Wu, S. Perales, B. Clevenger and R. S. Ruoff, *Nano Lett.*, 2012, **12**, 1806–1812.
17 J. Chmiola, C. Largeot, P. L. Taberna, P. Simon and Y. Gogotsi, *Science*, 2010, **328**, 480–483.
18 L. Hu, J. W. Choi, Y. Yang, S. Jeong, F. La Mantia, L.-F. Cui and Y. Cui, *Proc. Natl. Acad. Sci. U. S. A.*, 2009, **106**, 21490–21494.
19 V. L. Pushparaj, M. M. Shaijumon, A. Kumar, S. Murugesan, L. Ci, R. Vajtai, R. J. Linhardt, O. Nalamasu and P. M. Ajayan, *Proc. Natl. Acad. Sci. U. S. A.*, 2007, **104**, 13574–13577.
20 D. Pech, M. Brunet, H. Durou, P. Huang, V. Mochalin, Y. Gogotsi, P. L. Taberna and P. Simon, *Nat. Nanotechnol.*, 2010, **5**, 651–654.
21 A. G. Pandolfo and A. F. Hollenkamp, *J. Power Sources*, 2006, **157**, 11–27.
22 E. Frackowiak and F. Béguin, *Carbon*, 2001, **39**, 937–950.
23 E. Frackowiak and F. Béguin, *Carbon*, 2002, **40**, 1775–1787.
24 C. G. Liu, Z. Yu, D. Neff, A. Zhamu and B. Z. Jang, *Nano Lett.*, 2010, **10**, 4863–4868.
25 Y. Zhu, S. Murali, M. D. Stoller, K. J. Ganesh, W. Cai, P. J. Ferreira, A. Pirkle, R. M. Wallace, K. A. Cychosz, M. Thommes, D. Su, E. A. Stach and R. S. Ruoff, *Science*, 2011, **332**, 1537–1541.
26 X. Yang, J. Zhu, L. Qiu and D. Li, *Adv. Mater.*, 2011, **23**, 2833–2838.
27 H. M. Jeong, J. W. Lee, W. H. Shin, Y. J. Choi, H. J. Shin, J. K. Kang and J. W. Choi, *Nano Lett.*, 2011, **11**, 2472–2477.
28 X. Cao, Y. Shi, W. Shi, G. Lu, X. Huang, Q. Yan, Q. Zhan and H. Zhang, *Small*, 2011, **7**, 3163–3168.
29 V. Sridhar, H.-J. Kim, J.-H. Jung, C. Lee, S. Park and I.-K. Oh, *ACS Nano*, 2012, **6**, 10562–10570.
30 Z. Niu, J. Du, X. Cao, Y. Sun, W. Zhou, H. H. Hng, J. Ma, X. Chen and S. Xie, *Small*, 2012, **8**, 3201–3208.
31 M. G. Hahm, A. Leela Mohana Reddy, D. P. Cole, M. Rivera, J. A. Vento, J. Nam, H. Y. Jung, Y. L. Kim, N. T. Narayanan, D. P. Hashim, C. Galande, Y. J. Jung, M. Bundy, S. Karna, P. M. Ajayan and R. Vajtai, *Nano Lett.*, 2012, **12**, 5616–5621.

32 J. M. Miller, B. Dunn, T. D. Tran and R. W. Pekala, *J. Electrochem. Soc.*, 1997, **144**, L309–L311.
33 G. Yu, L. Hu, M. Vosgueritchian, H. Wang, X. Xie, J. R. McDonough, X. Cui, Y. Cui and Z. Bao, *Nano Lett.*, 2011, **11**, 2905–2911.
34 L. Yuan, X.-H. Lu, X. Xiao, T. Zhai, J. Dai, F. Zhang, B. Hu, X. Wang, L. Gong, J. Chen, C. Hu, Y. Tong, J. Zhou and Z. L. Wang, *ACS Nano*, 2012, **6**, 656–661.
35 C. Yuan, X. Zhang, L. Su, B. Gao and L. Shen, *J. Mater. Chem.*, 2009, **19**, 5772–5777.
36 Q. Wu, Y. Xu, Z. Yao, A. Liu and G. Shi, *ACS Nano*, 2010, **4**, 1963–1970.
37 L. Yuan, X. Xiao, T. Ding, J. Zhong, X. Zhang, Y. Shen, B. Hu, Y. Huang, J. Zhou and Z. L. Wang, *Angew. Chem., Int. Ed.*, 2012, **51**, 4934–4938.
38 H. Jiang, C. Li, T. Sun and J. Ma, *Nanoscale*, 2012, **4**, 807–812.
39 J. Zhang, J. Jiang, H. Li and X. S. Zhao, *Energy Environ. Sci.*, 2011, **4**, 4009–4015.
40 J. Jiang, Y. Li, J. Liu, X. Huang, C. Yuan and X. W. Lou, *Adv. Mater.*, 2012, **24**, 5166–5180.
41 M. Zhi, C. Xiang, J. Li, M. Li and N. Wu, *Nanoscale*, 2013, **5**, 72–88.
42 G. Xiong, K. P. S. S. Hembram, R. G. Reifenberger and T. S. Fisher, *J. Power Sources*, 2013, **227**, 254–259.
43 X. Lang, A. Hirata, T. Fujita and M. Chen, *Nat. Nanotechnol.*, 2011, **6**, 232–236.
44 L. Wei, N. Nitta and G. Yushin, *ACS Nano*, 2013, **7**, 6498–6506.
45 B. Radha, A. A. Sagade and G. U. Kulkarni, *ACS Appl. Mater. Interfaces*, 2011, **3**, 2173–2178.
46 T. Bhuvana and G. U. Kulkarni, *ACS Nano*, 2008, **2**, 457–462.
47 A. A. Sagade, B. Radha and G. U. Kulkarni, *Sens. Actuators, B*, 2010, **149**, 345–351.
48 B. Radha and G. U. Kulkarni, *Small*, 2009, **5**, 2271–2275.
49 B. Radha, S. H. Lim, M. S. M. Saifullah and G. U. Kulkarni, *Sci. Rep.*, 2013, **3**, 1078.
50 H. Nakanishi and B. A. Grzybowski, *J. Phys. Chem. Lett.*, 2010, **1**, 1428–1431.
51 S. W. Lee, J. Kim, S. Chen, P. T. Hammond and Y. S. Horn, *ACS Nano*, 2010, **4**, 3889–3896.
52 X. Jin, W. Zhou, S. Zhang and G. Z. Chen, *Small*, 2007, **3**, 1513–1517.
53 B. Radha, G. Liu, D. J. Eichelsdoerfer, G. U. Kulkarni and C. A. Mirkin, *ACS Nano*, 2013, **7**, 2602–2609.
54 T. Bhuvana and G. U. Kulkarni, *Int. J. Nanosci.*, 2011, **10**, 699–705.
55 M. Armand and J. M. Tarascon, *Nature*, 2008, **451**, 652–657.
56 S. D. Jones and J. R. Akridge, *Solid State Ionics*, 1996, **86–8**, 1291.
57 J. Lin, C. G. Zhang, Z. Yan, Y. Zhu, Z. W. Peng, R. H. Hauge, D. Natelson and J. M. Tour, *Nano Lett.*, 2013, **13**, 72–78.
58 C. Z. Meng, J. Maeng, S. W. M. John and P. P. Irazoqui, *Adv. Energy Mater.*, 2013, DOI: 10.1002/aenm.201301269.
59 M. D. Stoller and R. S. Ruoff, *Energy Environ. Sci.*, 2010, **3**, 1294–1301.
60 Z. Zolfaghari, F. Ataherian, M. Ghaemi and A. Gholami, *Electrochim. Acta*, 2007, **52**, 2806–2814.
61 A. L. M. Reddy, M. M. Shaijumon, S. R. Gowda and P. M. Ajayan, *J. Phys. Chem. C*, 2010, **114**, 658–663.
62 T. Brousse, M. Toupin and D. Bélanger, *J. Electrochem. Soc.*, 2004, **151**, A614–A622.
63 Z.-S. Wu, W. Ren, D.-W. Wang, F. Li, B. Liu and H.-M. Cheng, *ACS Nano*, 2010, **4**, 5835–5842.
64 Z. Fan, J. Yan, T. Wei, L. Zhi, G. Ning, T. Li and F. Wei, *Adv. Funct. Mater.*, 2011, **21**, 2366–2375.
65 M. S. Hong, S. H. Lee and S. W Kim, *Electrochem. Solid-State Lett.*, 2002, **5**, A227–A230.
66 Y. Shao, H. Wang, Q. Zhang and Y. Li, *J. Mater. Chem.*, 2013, **1**, 1245–1250.
67 X. Zhang, D. Zhao, Y. Zhao, P. Tang, Y. Shen, C. Xu, H. Li and Y. Xiao, *J. Mater. Chem. A.*, 2013, **1**, 3706–3712.
68 Z. Yu, B. Duong, D. Abbitt and J. Thomas, *Adv. Mater*, 2013, **25**, 3302–3306.